Fully self-consistent calculation of the electronic structure of *n*-type InAs accumulation layers

An-zhen Zhang, J. Slinkman,* and R. E. Doezema
Department of Physics and Astronomy, University of Oklahoma, Norman, Oklahoma 73019
(Received 15 February 1991)

The screening of an external electric field at the surface of a degenerate semiconductor is modified in narrow-band-gap materials due to "motional binding," where the confinement potential for surface-bound states depends on electron motion along the surface. A self-consistent calculation is presented that includes motional binding and treats both bound and mobile charge on the same footing. The calculation is applied to accumulation layers on *n*-type InAs and very good agreement is obtained with existing Shubnikov–de Haas data. The calculation is also used to predict intersubband spacings under conditions of motional binding.

I. INTRODUCTION

The interplay of bound and mobile charge in the scattering of an external electric field at the surface of a degenerate semiconductor was described in the work of Baraff and Appelbaum.[1] With *n*-type InAs as an example, they carried out a parametrized, self-consistent calculation, which successfully brought out the central features of screening in such degenerate systems. Because the full band structure of InAs was not included, however, it is not possible to use the Baraff-Appelbaum results for quantitative comparison to experimental data. Recently, we showed[2] that the screening properties are modified when the nonparabolicity of the band structure is taken into account because then the bound-state confinement potential depends on the motion along the semiconductor surface. This "motional binding" is a general feature of quantum wells with mass-mismatched barriers; in surface quantum wells (inversion or accumulation layers) on narrow-band-gap semiconductors, continuous spatial variation of the effective mass, as a result of the nonparabolicity, causes motional binding, as was recently shown by Doezema and Drew,[3] who employed a crude square-well approximation to simulate the effect, precluding a numerical comparison with data. For accumulation layers on degenerate, narrow-band-gap systems, a bound state is always motionally bound at the onset of occupation. At this threshold the delicate interplay between bound and continuum states is of particular interest and to fit the experimental results successfully in these regions would imply, for a calculation, that the screening is well understood indeed.

It is our purpose in this paper to present such a calculation with particular emphasis on motionally bound states. We use a four-band model for InAs and treat both bound and mobile charge on an equal footing. (Reisinger has carried out a similar calculation,[4] but ignored the motionally bound states.) In addition to fitting Schubnikov–de Haas data in the motional binding regime, we are able to predict the corresponding distribution of mobile charges and intersubband spacings over a range of bulk concentrations. We are also able to examine the relation between the existence of a motionally bound ground state and the "flatband" condition, which has not been unambiguously determined experimentally.

The elements of the problem are sketched in Fig. 1. The self-consistent potential $V(z)$ is assumed to support two bound states. The upper subband is shown motionally bound; i.e., it exists only for transverse wave vector k_t larger than k_{c1}. The Fermi level E_F, governed by the (degenerate) bulk electron density n, determines the Fermi wave vectors k_{F0} and k_{F1} for the ground state and first excited state. Both the ground-state and motionally bound electrons in the first excited state contribute to the screening and thus affect the mobile-state (continuum) electron density near the surface at $z=0$ (z is the coordinate into the semiconductor).

In Secs. II and III we discuss the theoretical frame-

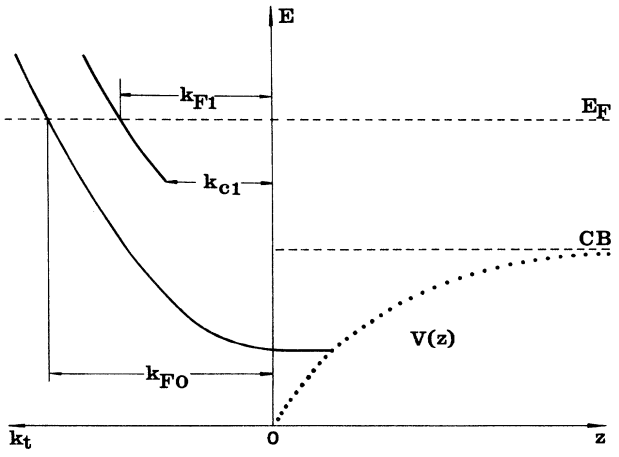

FIG. 1. Schematic potential well $V(z)$ and subband dispersion for an *n*-type InAs accumulation layer under motional binding conditions for the first excited state. For the zero and first subbands, the Fermi wave numbers (k_{F0} and k_{F1}) as well as the critical value of k_t for the first subband (k_{c1}) are indicated.

work and algorithms used in our calculation. Section IV contains an analysis of the numerical results together with a critical comparison with experiment, and Sec. V contains our conclusions and summary.

II. THEORETICAL FOUNDATION

To obtain a precise description of the accumulation layer in n-type InAs, we use the four-band model as described by Zawadski.[5] Our adaptation of this model is given in Sec. II A. In Sec. II B we present our method of achieving an exact, self-consistent solution of Poisson's equation. The calculation is developed at zero temperature, which Reisinger has shown[4] to be valid when comparing to data taken below 77 K.

A. Four-band model

For the range of electron concentrations considered here, the small effective mass at the InAs conduction-band edge ($m^*=0.0235m_0$, where m_0 is the free-electron mass) and large dielectric constant ($\epsilon=14.9$) combine to yield r_s values[6] in the range $0.1<r_s<0.5$. For this range of r_s, Baraff and Appelbaum[1] showed that many-body effects could be neglected relative to the Coulomb effects of principal interest in this work.

Following Zawadski,[5] we define a wave function for InAs of the Bloch form:

$$\Psi(\mathbf{r})=\sum_{l=1}^{4} f_l(z)u_l e^{-i\mathbf{k}_t\cdot\mathbf{r}} . \tag{1}$$

Here the index $l=1$ refers to the conduction band, which has s-like symmetry; the remaining l values designate the degenerate heavy- and light-hole bands and the split-off band, all of which have p-like symmetry. The u_l are the basis functions on the unit zinc-blende cell, and the f_l are envelope functions, which are to be determined in the calculation. The in-plane wave vector $\mathbf{k}_t$ is transverse to the direction of the applied electric field.

We apply the $\mathbf{k}\cdot\mathbf{p}$ method to the Schrödinger equation

$$\left[\frac{\mathbf{p}^2}{2m_0}+V_L(\mathbf{r})+V(z)\right]\Psi(\mathbf{r})=E\Psi(\mathbf{r}) , \tag{2}$$

where $V_L(\mathbf{r})$ is the lattice potential and $V(z)$, a function of the external field, is the screening potential to be determined self-consistently. Using the form (1) of the wave function, one finds that f_2, f_3, and f_4 can be written in terms of f_1, which we henceforth simply call f. This envelope function for the conduction band is found (for $m^*\ll m_0$) to satisfy

$$\left[-\frac{\hbar^2}{2m^*}\frac{\partial^2}{\partial z^2}+\frac{1}{E+E_g-V(z)}\frac{\partial V(z)}{\partial z}\frac{\hbar^2}{2m^*}\frac{\partial}{\partial z}+V(z)\left[1+\frac{2E}{E_g}-\frac{V(z)}{E_g}\right]\right]f(z)=\left[E\left[1+\frac{E}{E_g}\right]-\frac{\hbar^2k_t^2}{2m^*}\right]f(z) , \tag{3}$$

where E_g is the gap energy and an isotropic bulk dispersion relation has been assumed.

Solving Eq. (3) to determine both the bound and mobile states is of central importance. For bound states the bulk wave number k_z, is no longer a good quantum number. Instead, these states form a quasidiscrete spectrum, in k_t, of electric subbands, which we index with j. The corresponding eigenenergies are E_j.

B. Poisson's equation

In the presence of an external electric field in the z direction, both bound and mobile charges are distributed to screen the field. Self-consistency is obtained by finding simultaneous solutions to the Schrödinger equation, discussed above, and Poisson's equation:

$$\frac{\partial^2 V(z)}{\partial z^2}=-\frac{4\pi e}{\epsilon}\rho(z) . \tag{4}$$

The total charge density $\rho(z)$ is given in terms of the bound- and mobile-state wave functions $\Psi_{j,\mathbf{k}_t}(z)$ and $\Psi_{k_z,\mathbf{k}_t}(z)$, respectively:

$$\rho(z)=2e\sum_j\sum_{\mathbf{k}_t}\Psi^*_{j,\mathbf{k}_t}(z)\Psi_{j,\mathbf{k}_t}(z)+2e\sum_{\mathbf{k}_t}\sum_{k_z}\Psi^*_{k_z,\mathbf{k}_t}(z)\Psi_{k_z,\mathbf{k}_t}(z)-en . \tag{5}$$

In this approach, essentially similar to that of Baraff and Appelbaum,[1] the final term results from the fixed-background, donor-ion charge density and the summations are over all occupied bound and mobile states.

In Eq. (5) we convert the sums over $\mathbf{k}_t$ to a two-dimensional integral over $\mathbf{k}_t$ in the usual way. For bound states the integral runs from 0 to k_{Fj}, the Fermi wave

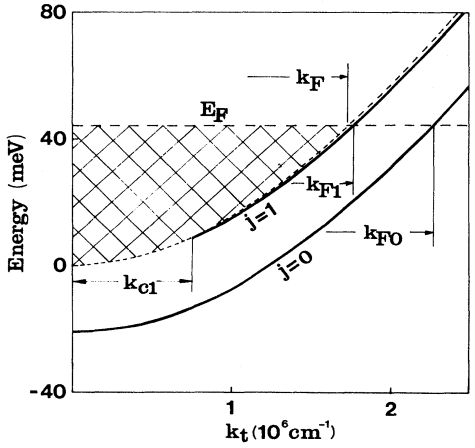

FIG. 2. Calculated dispersion relation E vs k_t, for $n=1.8\times10^{17}$ cm^{-3} when the first subband is motionally bound and occupied ($N_s=0.7\times10^{12}$ cm^{-2}). The hatched region delimits the area in k_t over which only occupied, mobile states can exist. Bound states exist only below the dashed curve defined by $k_z(k_t)=0$, i.e., the zero of the bulk wave-number component.

vector for the jth subband, except when the jth subband is occupied and motionally bound, in which case the lower limit corresponds to the cutoff k_{cj}. The integral for the mobile states runs from 0 to the bulk Fermi wave vector, $k_F=(3\pi^2 n)^{1/3}$, spanning the region of occupied states indicated in Fig. 2 by the crosshatched region. For computation it is convenient to replace the sum over k_z by an energy integral:

$$\sum_{k_z} \rightarrow \frac{1}{2\pi}\int_{E_{\min}(k_t)}^{E_F} dE \left[\frac{\partial k_z}{\partial E}\right]_{k_t}, \tag{6}$$

where the limits on E, for a given k_t, are from

$$E_{\min}(k_t)=\frac{-E_g}{2}+\left[\frac{E_g^2}{4}+\frac{E_g\hbar^2k_t^2}{2m^*}\right]^{1/2},$$

using the conduction-band dispersion relation, to the Fermi energy E_F. The donor-ion charge density can also be written[1] as an integral over k_t and k_z with the same limits as for the mobile states, allowing one finally to write

$$\rho(z)=\frac{2e}{(2\pi)^2}\sum_j \int_0^{k_F j} dk_t\, k_t \Psi^*_{j,k_t}(z)\Psi_{j,k_t}(z)+\frac{2e}{(2\pi)^2}\int_0^{k_F} dk_t\, k_t \int_{E_{\min}(k_t)}^{E_F} dE \left[\frac{\partial k_z}{\partial E}\right]_{k_t}[\Psi^*_{E,k_t}(z)\Psi_{E,k_t}(z)-1]. \tag{7}$$

The total electron sheet density $N_s=\int_0^\infty \rho(z)$ is given through Poisson's equation by the slope of the potential at the interface:

$$N_s=\frac{\epsilon}{4\pi}\left.\frac{dV(z)}{dz}\right|_{z=0}. \tag{8}$$

It is clear from expression (7) that N_s is composed of a bound and a mobile contribution:

$$N_s=\sum_j N_{sj}^b+N_s^m, \tag{9}$$

where N_{sj}^b is the density of bound electrons occupying subband j and N_s^m is the mobile-state contribution.

III. COMPUTATIONAL ALGORITHMS

The goal of our self-consistent calculation is to find bound and mobile charge densities which simultaneously satisfy the Poisson and Schrödinger equations through the potential function $V(z)$, which is consistent with the applied electric field at the interface. We use an iterative method to achieve self-consistency. In this section we describe the general features of our iteration scheme. We next detail the solution of Eq. (3) separately for the bound and mobile states. We then discuss the computation of the charge density $\rho(z)$ and the solution of Eq. (4). For additional details, the reader is referred to a dissertation.[7]

A. Iteration scheme

The Fermi energy E_F is determined in degenerate n-type InAs by the concentration n. The relationship $E_F(n)$ is fixed by the conduction-band dispersion relation

$$E=-\frac{E_g}{2}+\left[\frac{E_g^2}{4}+\frac{E_g\hbar^2k_t^2}{2m^*}\right]^{1/2},$$

with $k_t=k_F$. The value of the potential at the interface, $V(0)$, is also taken as an input parameter. The N_s value resulting from a given choice of $V(0)$ is an output quantity through Eq. (8). For $z\rightarrow\infty$, deep in the bulk, we assume that both $V(z)$ and dV/dz vanish. To start off the iteration, we use an initial guess for the potential function, denoted by $V_1(z)$. Following Refs. 1 and 4, we express this function as a sum of exponentials:

$$V_1(z)=\sum_{p=1}^{5}\beta_p e^{-z/p\lambda}. \tag{10}$$

In practice, we found that, even in the most highly nonlinear regimes, only one or two terms in this expression were usually necessary. A single iteration through the entire algorithm required first a numerical integration of Eq. (3). With the resulting wave functions, the charge density $\rho(z)$ could then be constructed from Eq. (7). Poisson's equation (4) was then solved, and the result $V_{\text{out}}(z)$ was compared point by point to the initial potential $V_{\text{in}}(z)$ used to solve Eq. (3) for the iteration.

B. Bound-state computation

A bound state satisfies the condition,

$$E_j(\mathbf{k}_t)<V(z_{\max}),$$

where $E_j(\mathbf{k}_t)$ is the eigenvalue for the jth subband corresponding to motion in the z direction and $z_{\max}$ specifies a point deep in the bulk. We typically choose $z_{\max}=16/k_F$, i.e., much larger than the depth of the surface potential, which is of the order of $\lambda\sim 1/k_F$. We assume that the bound-state wave functions $f^b_{j,k_t}(z)$ vanish at the surface, $z=0$. The asymptotic form of the wave functions for $z\gg 1/k_F$ was chosen to be a decaying exponential characterized by a z-component wave number k_z determined from the bulk dispersion relation

$$k_z=\left\{\frac{2m^*}{\hbar^2}\left[E\left[1+\frac{E}{E_g}\right]\right]-k_t^2\right\}^{1/2}. \tag{11}$$

A fourth-order Runge-Kutta scheme[8] is used to integrate Eq. (3) from $z_{\max}$ to $z=0$ for a given value of k_t. The correct bound-state energy E_j and wave function are obtained when the boundary conditions on $f^b_{j,k_t}(z)$ is found

at $z=0$. The normalization requirement is applied to the total bound-state wave function $\Psi_{j,k_t}(z)$.

C. Mobile-state computation

A mobile state satisfies the condition

$$E_{k_z}(\mathbf{k}_t) > V(Z_{\max}) ,$$

where the energy for z motion, $E_{k_z}(\mathbf{k}_t)$, is quasicontinuous and k_z is a good quantum number, related to E and k_t through Eq. (11). There are two possible asymptotic solutions for the mobile-state wave functions $f_{\mathbf{k}}^{m}(z)$, which we denote by $f_{\mathbf{k}}^{mc}(z)$ and $f_{\mathbf{k}}^{ms}(z)$, as $z \rightarrow z_{\max}$:

$$f_{\mathbf{k}}^{mc}(z_{\max}) = \cos(k_z z_{\max}) \tag{12a}$$

and

$$f_{\mathbf{k}}^{ms}(z_{\max}) = \sin(k_z z_{\max}) . \tag{12b}$$

Both $f_{\mathbf{k}}^{mc}(z)$ and $f_{\mathbf{k}}^{ms}(z)$ are determined for all z in general by integrating Eq. (3) from the starting values of Eqs. (12a) and (12b). We then form the linear combination:

$$f_{\mathbf{k}}^{m}(z) = a(\mathbf{k}_t,E) f_{\mathbf{k}}^{ms}(z) + b(\mathbf{k}_t,E) f_{\mathbf{k}}^{mc}(z) . \tag{13}$$

Imposing the boundary condition at $z=0$ then yields the wave-function phase corresponding to an eigenstate:

$$\eta(\mathbf{k}_t,E) = -\tan^{-1}\left[\frac{b(\mathbf{k}_t,E)}{a(\mathbf{k}_t,E)}\right] . \tag{14}$$

Box normalization[1] on the interval $L_z = z_{\max}$ is imposed on the total mobile-state wave function $\Psi_{E,\mathbf{k}_t}(z)$.

D. Self-consistent determination of $V(z)$

The bound- and mobile-state wave functions obtained above are used to compute the total charge density $\rho(z)$ with Eq. (7). Poisson's equation [Eq. (4)] is then solved with the boundary conditions $V(z_{\max})=0$ and $(dV/dz)(z_{\max})=0$ and with the initially fixed value $V(0)$, an input parameter. A finite-difference, successive-overrelaxation method[8] was employed to determine $V(z)$ for all z in a given iteration i. This newly determined potential $V_i^{\text{out}}(z)$ is then compared to the potential $V_i(z)$ used to solve Eq. (3) in the ith iteration. For n selected values z_n between $z=0$ and $z=z_{\max}$, we form the ratio

$$\delta_V = \left| \frac{V_i^{\text{out}}(z_n) - V_i(z_n)}{V(0)} \right| . \tag{15}$$

Our convergence criterion was $\delta_V \leq 10^{-3}$. To form the input potential for the $(i+1)$th iteration, only a fraction of the output potential was used:

$$V_{i+1}(z) = (1-f_{i+1}) V_i(z) + f_{i+1} V_i^{\text{out}}(z) . \tag{16}$$

On each iteration the fraction f_{i+1} was chosen in the range 0.01–0.2. This technique is a variation of the extrapolated convergence method.[9]

In each iteration the calculation of the Jacobian $(\partial k_z/\partial E)_{k_t}$, in Eq. (7), is of particular importance. The direct but computationally intense method is to calculate $k_z(z,k_t,E)$:

$$k_z(z,k_t,E) = -i \frac{\partial \Psi_{E,k_t}(z)}{\partial z} , \tag{17}$$

and then form the derivative numerically. We found that an acceptable trade-off between precision and speed is to approximate the derivative by using the bulk relation of Eq. (11) and replacing E with $E - V_i(z)$ to obtain an analytical expression for $(\partial k_z/\partial E)_{k_t}$.

For a reasonable initial guess of $V_1(z)$, convergence was typically obtained in 10–20 iterations, except in the case of motional binding, when typically 50 iterations were needed.

IV. RESULTS

A. Comparison to experiment

A very sensitive test of our calculation is provided by a comparison to Shubnikov–de Haas (SdH) data. The frequency of SdH oscillations, B_f^j, corresponding to the jth subband and given by $B_f^i = c\hbar k_{Fj}^2/2e$, is usually a measure of the subband occupation N_{sj}, because N_{sj} is given by $k_{Fj}^2/2\pi$. However, if the subband is occupied and motionally bound, N_{sj} is given by $(k_{Fj}^2 - k_{cj}^2)/2\pi$, where k_{cj} is the cutoff transverse wave vector.[3] Thus, in the regime of motional binding, the SdH frequency is "pinned" to k_{Fj}^2, which is essentially constant in this regime. This pinning is the signature of motional binding in SdH experiments.[3] We wish for our calculation to match the

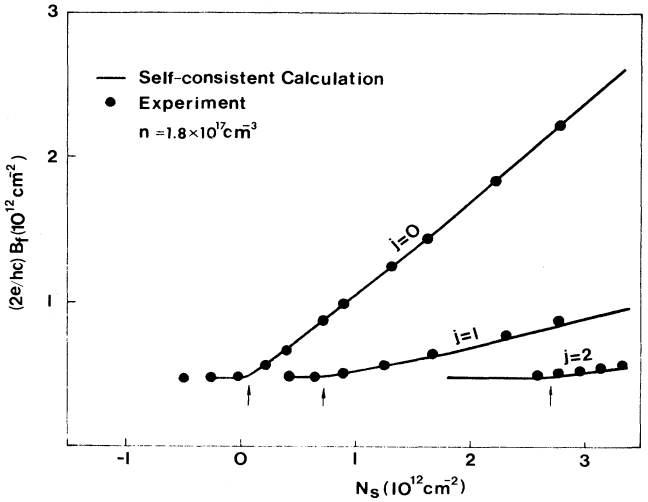

FIG. 3. Comparison of our calculated Shubnikov–de Haas frequency B_f vs total surface carrier density N_s to the data of Radentsev *et al.* (Ref. 10) for bulk density 1.8×10^{17} cm^{-3}. The arrows indicate the termination of motional binding ($k_{cj}=0$) for each subband. All experimental points were slightly shifted in N_s as discussed in the text.

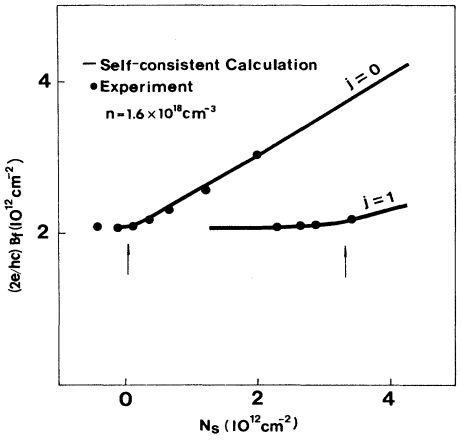

FIG. 4. Comparison of calculated vs experimental B_f vs N_s for heavy bulk density 1.6×10^{18} cm^{-3}. All notation and scales are as in Fig. 3.

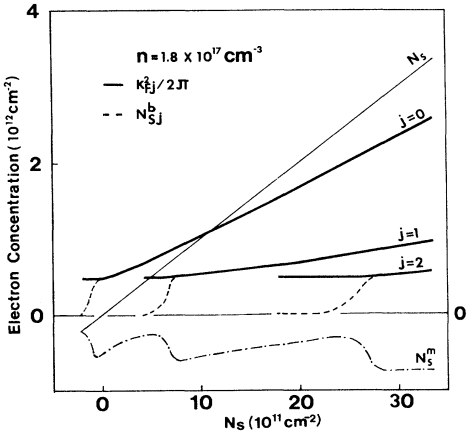

FIG. 5. Calculated subband-electron concentrations N_{sj}^b and mobile surface-electron concentration N_s^m as a function of total surface-electron concentration N_s for bulk concentration 1.8×10^{17} cm^{-3}. In the absence of motional binding, N_{sj}^b is identical to $k_{Fj}^2/2\pi$.

measured SdH frequencies over the whole range of surface-electron density, but especially in the region of motional binding.

Figures 3 and 4 compare our predicted SdH frequencies to experiment. We have used the data of Radentsev *et al.*[10] for a moderately doped ($n=1.8\times10^{17}$ cm^{-3}) and a more heavily doped ($n=1.6\times10^{18}$ cm^{-3}) sample. The zeros of the experimental curves have been slightly shifted to make the data for the ground state coincide with the theoretical prediction. The shift is necessary because of the difficulty of determining the "flatband" or $N_s=0$ condition experimentally. The small size of the needed shift ($\approx1\times10^{11}$ cm^{-2}) indicates that the empirical determination of the flatband used for experimental data[10,11] is nearly correct. In general, the agreement between theory and experiment is excellent. In the motional binding regime for the ground state, the calculation converges so slowly that it was only possible to verify that the ground state is indeed motionally bound and occupied at the N_s values indicated by the SdH data. It is likely that the motional binding regime persists to even lower N_s values than indicated by experiment. (The excited subbands show this in Figs. 3 and 4; both the N_s independence of B_f^j and the decreasing subband occupancy can contribute to loss of experimental signal in this regime.) The interesting region of negative N_s values where the ground state is motionally bound is discussed in more detail below.

B. Properties of the screening layer

Assured by the good agreement with the SdH data that we have found the correct screening potential, we can now calculate quantities of interest which are not directly accessible in the SdH experiments.

The first of these quantities is the subband occupancy N_{sj}. It is not accessible to the experiment in the motional binding regimes, where it is no longer given by $k_{Fj}^2/2\pi$. Figures 5 and 6 show that with decreasing N_s the subband occupation densities in these regions fall rapidly from the fully bound occupancy when $k_{cj}=0$ to zero when $k_{cj}=k_{Fj}$. At the same time, with decreasing N_s, the deficit of mobile charge density in the surface region decreases to compensate for the rapid loss of bound charge. Aside from small adjustments in the motional binding regions, the self-consistent potential (seen for several N_s values in Fig. 7) varies smoothly with N_s. The small adjustments are evident in Fig. 8, where we show how the depth of the well, $V(0)$, and the subband edges vary with N_s. These adjustments reflect the changeover from screening by mobile charges to screening by bound

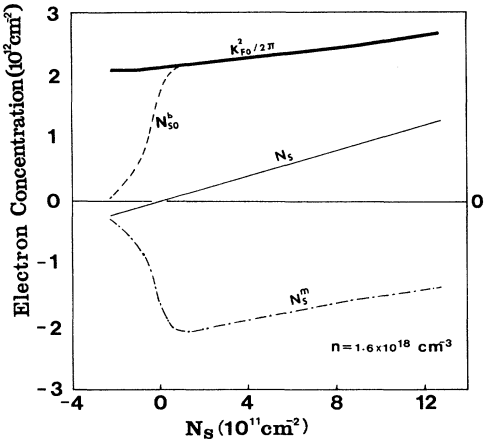

FIG. 6. Calculated ground-state subband concentration N_{s0}^b and mobile surface-electron concentration N_s^m vs total surface-electron concentration N_s for bulk concentration 1.6×10^{18} cm^{-3}. In the absence of motional binding, N_{s0}^b is identical to $k_{F0}^2/2\pi$.

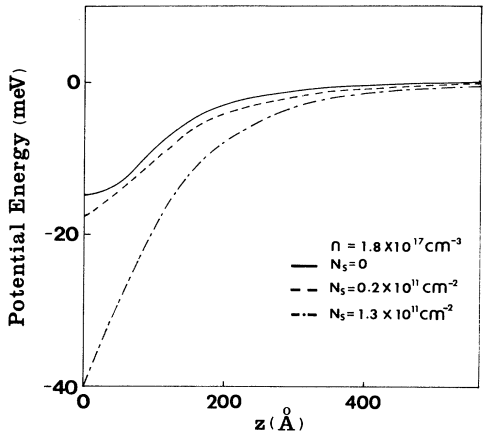

FIG. 7. Calculated self-consistent potential $V(z)$ as a function of distance into the semiconductor for $n=1.8\times10^{17}$ cm^{-3}. Note the existence of a binding potential for $N_s=0$.

charges in the motional binding regions. The mobile charge can only screen on a length scale of order $1/k_F$, where k_F is the bulk Fermi wave vector, whereas the bound charge screens an external field over a distance determined by the bound-state wave-function extent.

The interplay between the mobile and bound charges in screening is brought out in Fig. 9, where the bound and mobile charge densities are plotted as a function of distance from the surface. The bound charge density $\rho^b(z)$ and mobile charge density $\rho^m(z)$ are given by the first and second terms of Eq. (7), respectively. The mobile charge density is a measure of the deviation from charge neutrality which holds in the bulk of the semiconductor. The response of the mobile charges to the onset of (motionally bound) subband occupation shows the behavior expected from the formation of an "orthogonality hole," discussed

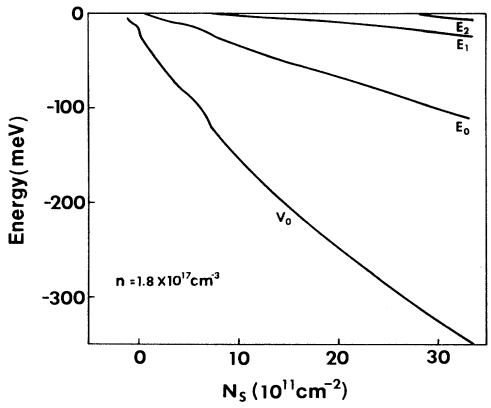

FIG. 8. Subband energies (for $k_t=0$) and potential $V(0)$ at the sample surface as a function of total surface-electron concentration for $n=1.8\times10^{17}$ cm^{-3}.

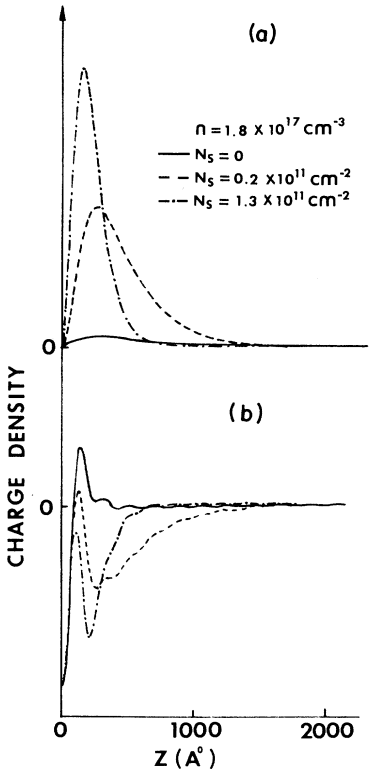

FIG. 9. (a) Bound charge density $\rho^b(z)$ for the ground-state subband as a function of distance into the semiconductor for several N_s values. For $N_s=0$ the state is motionally bound. (b) Mobile charge density $\rho^m(z)$ as a function of distance into the semiconductor for the same N_s values as in (a).

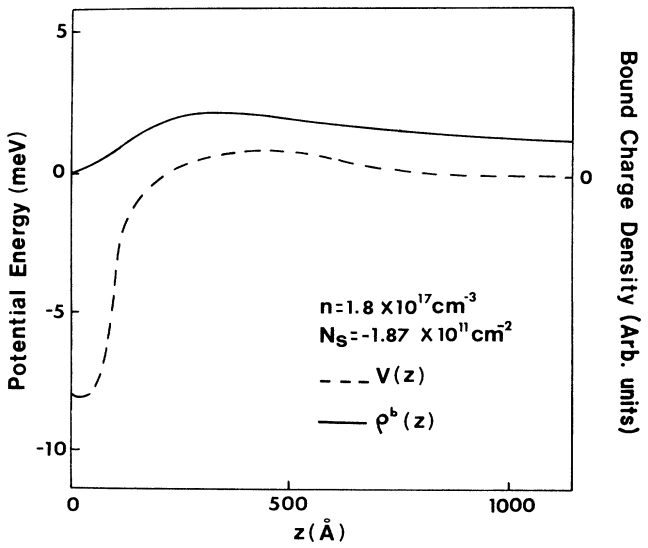

FIG. 10. Self-consistent potential and ground-state charge density distribution in the $N_s<0$ regime. The scale of the charge density is magnified relative to that of Fig. 9: The peak of the bound charge density for $N_s=-1.87\times10^{11}$ cm^{-2} is nearly an order of magnitude less than the peak for $N_s=0$ shown in Fig. 9(a).

by Baraff and Appelbaum,[1] which is caused by the requirement of orthogonality between bound- and mobile-state wave functions. It is also gratifying to note that the mobile charge density exhibits the expected Friedel oscillations with period $\sim 2/k_F$.

In Fig.10 we show the self-consistent potential and density distributions near $N_s=0$, the flatband condition. At $N_s=0$ the potential is flat at the surface, i.e., $dV/dz=0$ at $z=0$. However, as discussed by Baraff and Appelbaum,[1] the positive ionic layer caused by vanishing electron wave functions at $z=0$ induces an attractive self-consistent potential well at the surface which can support a bound state. This bound state persists into the negative N_s region ($dV/dz<0$ at $z=0$) as a motionally bound state. To determine the exact N_s where the state disappears would require extreme computational precision.

C. Intersubband spacings

A final quantity of interest is the intersubband spacing, which can be measured spectroscopically without a depolarization shift in narrow-gap systems.[12] Measurements outside the motional binding regimes have been performed[13,4] which are in good agreement with the predictions of Reisinger's self-consistent calculation.[4] Here we are particularly interested in predicting transition energies in the motional binding regimes.

Because of bulk nonparabolicity, the subband spacings in InAs vary with k_t. Allowed transitions $i \rightarrow j$ occur over a range of k_t: from the k_t value, where subband j coincides with the Fermi level (or the onset of motional binding for subband j if it occurs at an energy higher than the Fermi energy), to the k_t value, where subband i crosses the Fermi level. Possible $0 \rightarrow 2$ transitions (for $T=0$) are shown in Fig. 11 corresponding to total N_s values in the motional binding regime of subband $j=2$. The line broadening implied by the variation of the spacing with k_t is generally less than the observed[13] width of intersubband transitions in InAs, and so we can safely take the average value of the intersubband spacing in the allowed k_t range as the characteristic intersubband spacing for a given N_s value. Figure 11 also indicates that once, with decreasing N_s, subband j is not occupied ($k_{cj} \geq k_{Fj}$), the intensity of the $i \rightarrow j$ transition will smoothly decrease to zero (in which case $k_{cj} \geq k_{Fi}$). The predicted transition energies are shown in Fig. 12 for the

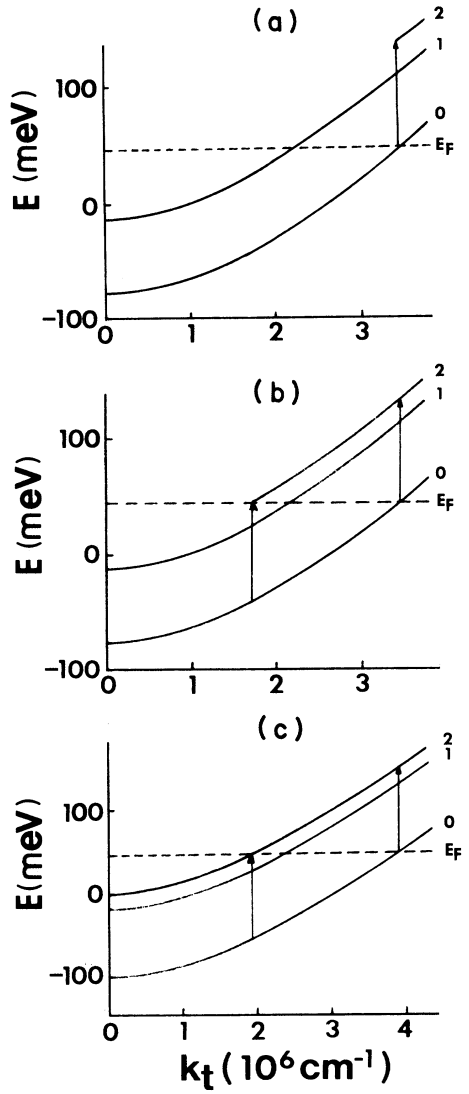

FIG. 11. Evolution of subband dispersion in the motional binding regime for the $j=2$ subband. Three N_s values are shown for $n=1.8\times10^{17}$ cm^{-3} corresponding to (a) first allowed transition ($T=0$) from the ground state to motionally bound subband 2, (b) saturation of k_t range of allowed transitions from the ground state to motionally bound subband 2 (allowed transitions are in the range between the two arrows), and (c) subband 2 fully bound.

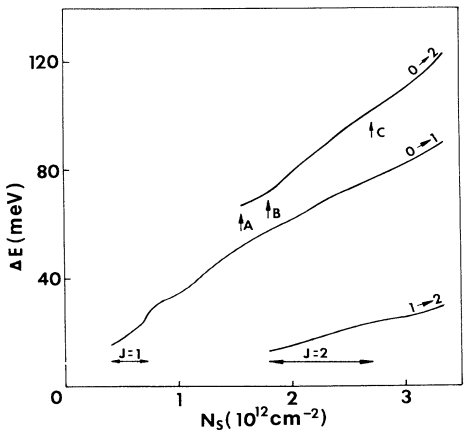

FIG. 12. Intersubband transition energies vs N_s for $n=1.8\times10^{17}$ cm^{-3}. The motional binding regimes (occupied states only) are indicated by horizontal arrows for subbands 1 and 2. The values labeled A, B, and C correspond to the conditions shown in Fig. 11.

same bulk concentration as for Fig. 11, and the N_s values corresponding to the three situations depicted in Fig. 11 are marked. Outside the regions of motional binding, we find agreement with the results of Reisinger's calculation. An experimental study of the motional binding regimes with intersubband resonance is in progress.[14]

V. CONCLUSIONS

We have presented a self-consistent calculation of the accumulation layer on *n*-type InAs which is in excellent agreement with existing SdH data, in particular in the regimes of surface-carrier density where motional binding occurs. The calculation allowed us to examine the interplay between bound and mobile carriers in screening external fields. Good agreement is found with the picture of screening in degenerate semiconductors presented by Baraff and Appelbaum. The inclusion of motional binding into the calculation removes discontinuities in the shape of the self-consistent potential at the onset of subband occupancy. Finally, we are able to use the calculation to predict intersubband transition energies. Outside the regions of motional binding, the results agree with the work of Reisinger. A study of intersubband resonance under conditions of motional binding is highly desirable and would provide a sensitive additional test of our calculation.

ACKNOWLEDGMENTS

It is a pleasure to thank Yousong Zhang for useful discussions and to thank Lihe Bu for carrying out some of our final calculations. We are also grateful to Bruce Mason and Frank Stern for valuable discussions and encouragement. One of us (J.S.) is indebted to IBM for granting a leave of absence to complete this work. This work was supported by National Science Foundation (NSF) Grant Nos. RII-86-10676 and DMR-8912686.

*Permanent address: IBM General Technology Division, Essex Junction, VT 05452.

[1]G. A. Baraff and J. A. Appelbaum, Phys. Rev. B **5**, 475 (1971).
[2]J. Slinkman, Ah-zhen Zhang, and R. E. Doezema, Phys. Rev. B **39**, 1251 (1989).
[3]R. E. Doezema and H. D. Drew, Phys. Rev. Lett. **57**, 762 (1986).
[4]H. Reisinger, doctoral dissertation, Technische Universität München, 1983.
[5]W. Zawadski, J. Phys. C **16**, 229 (1983).
[6]See, for example, p. 620 of T. Ando, A. B. Fowler, and F. Stern, Rev. Mod. Phys. **54**, 437 (1982).
[7]An-zhen Zhang, Ph.D. dissertation, University of Oklahoma, 1990.
[8]W. H. Press, B. P. Flannery, S. A. Teukolsky, and W. T. Vetterling, *Numerical Recipes: The Art of Scientific Computing* (Cambridge University Press, Cambridge, England, 1987).
[9]F. Stern, J. Comput. Phys. **6**, 56 (1970).
[10]V. F. Radantsev, T. I. Derybina, L. P. Zverev, G. I. Kulaev, and S. S. Khomutova, Zh. Eksp. Teor. Fiz. **91**, 1016 (1986) [Sov. Phys.—JETP **64**, 598 (1986)].
[11]H. Reisinger, H. Schaber, and R. E. Doezema, Phys. Rev. B **24**, 5690 (1981).
[12]K. Wiesinger, H. Reisinger, and F. Koch, Surf. Sci. **113**, 102 (1982).
[13]H. Reisinger and F. Koch, Solid State Commun. **37**, 429 (1981).
[14]Y. Zhang, A. Zhang, J. Slinkman, and R. E. Doezema, this issue, Phys. Rev. B **44**, 10 749 (1991).